Particuology 49 (2020) 191–204

Contents lists available at ScienceDirect

Particuology

journal homepage: www.elsevier.com/locate/partic

Numerical analysis and experimental validation of hydrodynamics of a thin bubbling fluidized bed for various particle-size distributions using a three-dimensional dense discrete phase model

Abolhasan Hashemisohi [a], Lijun Wang [b,c,*], Abolghasem Shahbazi [b,c], Hossein Amini [a]

[a] Department of Computational Science and Engineering, North Carolina A&T State University, Greensboro, NC 27411, USA
[b] Department of Natural Resources and Environmental Design, North Carolina A&T State University, Greensboro, NC 27411, USA
[c] Department of Chemical, Biological, and Bioengineering, North Carolina A&T State University, Greensboro, NC 27411, USA

ARTICLE INFO

Article history:
Received 10 January 2018
Received in revised form 18 April 2019
Accepted 29 April 2019
Available online 2 July 2019

Keywords:
Computational fluid dynamics
Fluidization
Particle size distribution
Hybrid Eulerian–Lagrangian model
Dense discrete phase model
Wall friction

ABSTRACT

A dense discrete phase model combined with the kinetic theory of granular flows was used to study the bubbling characteristics and segregation of poly-dispersed particle mixtures in a thin fluidized bed. Our simulations showed that in using the hybrid Eulerian–Lagrangian method, the common use of one computational cell in the thickness direction of the thin bed does not predict wall friction correctly. Instead, a three-cell discretization of the thickness direction does predict the wall friction well but six cells were needed to prevent overprediction of the bed expansion. The change in specularity factor (SF) of the model not only affected the predictions of the velocity of particles, but also had a considerable impact on their flow pattern. A decrease in SF, which decreases wall friction, showed an over-prediction in the size of bubbles, particle velocities, and void fraction of the bed, and led to a shift in the circulation center toward the bottom of the bed. The segregation of the Geldart B particles was studied in the narrow range from 400 to 600 μm with a standard deviation less than 10% of the average diameter. Simulations showed that large particles accumulated close to the distributor at the bottom of the bed and the center of the bed, but small particles moved towards the wall and top surface. The decrease in the mean particle size and spread in shape of the distribution improves mixing by up to 30% at a superficial gas velocity of around 2.5 times the minimum fluidization velocity. Log-normal mixtures with a small proportion of large particles had the most uniform distribution with a thin layer of jetsam forming at the bottom of the bed. Finally, experimental verification of the segregation and mixing of polydisperse particles with narrow size distribution is suggested.

Introduction

Fluidized bed reactors are widely used in many industrial processes such as fluidized catalytic cracking, and coal\biomass combustion and gasification (Geldart, 1969; Kunii & Levenspiel, 1991a). The vigorous mixing of solids and gas in fluidized bed reactors may attain high heat and mass transfer rates (Kunii & Levenspiel, 1991b). However, designing and operating fluidized bed reactors is challenging because of the complex hydrodynamics and resultant particle and bubble behaviors. With recent advances in computer technology, mathematical modeling and computer simulation can be used as an inexpensive and effective tool to predict the hydrodynamic behaviors of a fluidized bed (Kunii & Levenspiel, 1991a; Loha, Gu, De Wilde, Mahanta, & Chatterjee, 2014).

Modeling of the hydrodynamics of fluidized bed systems are classified under three major approaches: the two-phase theory of fluidization, the Eulerian–Eulerian (E–E) model, and the Eulerian–Lagrangian (E–L) model. The empirical correlations for the determination of hydrodynamic parameters based on the two-phase theory of fluidization must be modified for different conditions and regimes in fluidization (Davidson & Harrison, 1966; Hashemi Sohi, Eslami, Sheikhi, & Sotudeh-Gharebagh, 2012; Sheikhi, Sotudeh-Gharebagh, Eslami, & Sohi, 2012). The E–E approach gives a realistic prediction of hydrodynamic properties such as bubble formation, and spatial and temporal changes in the volumetric fraction of the solid phase. Filtered and energy

* Corresponding author at: Department of Natural Resources and Environmental Design, North Carolina A&T State University, Greensboro, NC 27411, USA.
E-mail address: lwang@ncat.edu (L. Wang).

https://doi.org/10.1016/j.partic.2019.04.001
1674-2001/

minimization multi-scale approaches were further developed to improve the sub-grid predictions when a coarse grid was used during the computational fluid dynamics (CFD) simulations (Hong et al., 2018; Igci & Sundaresan, 2011; Igci, Andrews, Sundaresan, Pannala, & O'Brien, 2008; Shi, Wang, & Li, 2011). However, an E–E model is unable to track information such as residence time and shrinkage and growth of individual particles during reactions (Arastoopour, Gidaspow, & Abbasi, 2017).

Among several E–L approaches, the soft-sphere discrete element method (DEM) gives the most accurate collision resolution and trajectory of the particles (Deen, Annaland, Van der Hoef, and Kuipers (2007); Hoomans, Kuipers, Briels, & van Swaaij, 1996; Schwartz, Richardson, & Michel, 2012; Tsuji, Kawaguchi, & Tanaka, 1993). However, as the simulations with the DEM are time consuming, the DEM is thus suitable for the simulation of small-scale fluidized beds or industrial scale fluidized beds with Geldart group D particles (Xu et al., 2011). Efforts have been directed to simplify the collision between particles and to reduce the number of particles by grouping them into parcels (Andrews & O'Rourke, 1996; Benyahia & Galvin, 2010; Hoomans et al., 1996; Lu, Benyahia, & Li, 2017; Lu, Gopalan, & Benyahia, 2017; Lu, Morris, Li, & Benyahia, 2017; Ozel, Kolehmainen, Radl, & Sundaresan, 2016; Snider, 2007). The lattice-Boltzmann method was coupled with the DE M to simulate the fluidized beds and some interesting results were reported in the literature (Third, Chen, & Müller, 2016; Xiong, Madadi-Kandjani, & Lorenzini, 2014).

A hybrid E–L approach by grouping particles into parcels in the E–L frame was found to be computationally feasible for the simulation of fluidized bed reactors with polydispersed bed material in industrial scales (Adamczyk et al., 2015; Snider, 2007; Snider, Clark, & O'Rourke, 2011). In the original hybrid E–L approach, the parcel properties were mapped into the Eulerian grid to calculate their interactions based on isotropic inter-particle stress (Harris & Crighton, 1994) and mapped back to the parcel positions (Andrews & O'Rourke, 1996; Snider, O'rourke, & Andrews, 1998). This hybrid E–L method was used to simulate large scale fluidized beds with a reasonable computational time and different results were reported (Fotovat, Abbasi, Spiteri, de Lasa, & Chaouki, 2015; Snider, 2007). Later, another type of E–L CFD model, called the dense discrete phase model (DDPM), was introduced that modeled the interactions between particles using a solid stress from the kinetic theory of granular flows (Popoff & Braun, 2007). In this DDPM, the collision term contains only the normal pressure instead of the complete stress tensor. Our previous study showed that the total stress tensor should be used to predict the formation of bubbles accurately (Hashemisohi, Wang, & Shahbazi, 2019). Cloete, Johansen, and Amini (2012) also studied the effect of the collision term for the simulation of dilute systems with periodic boundary conditions.

Simulations of circulating fluidized beds of boilers and coal gasifiers have confirmed the computational benefits using the DDPM approach (Adamczyk et al., 2014a, 2014b, 2014c, 2015). The simulation of a bubbling fluidized bed using the DDPM approach required less computational time with a good grid independency, compared to the E–E approach (Cloete, Johansen, Braun, Popoff, & Amini, 2011; Cloete et al. 2012). However, there was a substantial difference in the prediction of bubble formation using two-dimensional (2D) and three-dimensional (3D) simulations but minor effects in the prediction of pressure drop and bed expansion (Cloete et al., 2011). However, these simulations were validated with macro-scale properties of a fluidized bed, such as pressure drop and bed expansion, but lacked the details in the prediction of micro-scale and meso-scale properties of a fluidized bed including bubble size, frequency, solid flow patterns, velocity of circulation of particles at different operating conditions, and particle size distributions.

Pseudo- 2D fluidized beds (the third dimension of which is much smaller than the other two dimensions) have been extensively used to study the hydrodynamic properties in a fluidized bed by non-invasive experimental methods called particle image velocimetry and digital image analysis (Cloete et al., 2011; Hernández-Jiménez, Sánchez-Delgado, Gómez-García, & Acosta-Iborra, 2011; Sánchez-Delgado, Marugán-Cruz, Soria-Verdugo, & Santana, 2013). CFD models can be validated by comparing the 2D or 3D predictions and experimental results obtained from pseudo-2D beds. The effects of back and front wall friction on the velocity of particles and bubble size in a pseudo-2D fluidized bed have been studied using E–E and E–L CFD approaches (Altantzis, Bates, & Ghoniem, 2015; Li, Grace, & Bi, 2010). The effects of bed thickness on 3D flow behaviors and segregation in a pseudo-2D fluidized was studied using the CFD-DEM approach (Li, Gopalakrishnan, Garg, & Shahnam, 2012). Cloete et al. (2015) studied the effect of frictional pressure, geometry and wall friction in a pseudo-2D fluidized bed using a TFM model. Liang, Zhang, Li, and Lu (2014) simulated a pseudo-2D fluidized bed using the MP-PIC method and successfully predicted particle velocities but not the flow pattern using only one cell in the thickness direction. Wang et al. (2015) studied the particle size distribution in a 2D circulating fluidized bed using a CPFD model and they obtained good predictions of overall flow patterns in dilute systems. Cloete and Amini (2016) compared the effects of gas velocity and particle size on the bed expansion in a pseudo-2D fluidized bed using the TFM and DDPM models. Information is lacking about the effect of wall friction on a pseudo-2D fluidized bed in simulations using the DDPM model and the corresponding coefficients in the DDPM model that take into account the effect of wall friction. Also, there is a critical need to validate the DDPM model in the prediction of bubbling characteristics and flow patterns.

Polydispersity is a very important parameter affecting hydrodynamic, mixing, segregation, and mass and heat transfer especially between the bubble and emulsion phase (Geldart, 1969, 1972). The studies reported in the literature show that adding fine particles was beneficial in improving the efficiency of a fluidized bed reactor (Geldart, 1972; Grace & Sun, 1991; Joseph, Leboreiro, Hrenya, & Stevens, 2007; Khoe, Ip, & Grace, 1991). Numerous experimental and simulation studies have focused on the segregation of polydisperse systems using binary mixtures or solid fuel trajectory and different mixing indices have been defined (Beetstra, van der Hoef, & Kuipers, 2007; Di Renzo, Di Maio, Girimonte, & Formisani, 2008; Fan & Wang, 1975; Feng, Xu, Zhang, Yu, & Zulli, 2004; Fotovat et al., 2015; Hernández-Jiménez, García-Gutiérrez, Soria-Verdugo, & Acosta-Iborra, 2015; Hoomans, Kuipers, & van Swaaij, 2000; Huilin, Yunhua, Ding, Gidaspow, & Wei, 2007; Joseph et al., 2007; Monazam, Breault, Weber, & Layfield, 2017; Peng, Doroodchi, Alghamdi, & Moghtaderi, 2013). However, industrial fluidized beds contain materials with continuous particle size distribution. Gauthier, Zerguerras, and Flamant (1999) have reported that powders with a Gaussian distribution have the same minimum fluidization velocity as their average uniform-sized powders whereas binary and flat-distribution mixtures segregate. Segregation has also been shown to increase with increasing width in the particle-size distribution, bed height, mean size, and gas velocity, and with decreasing size in fines (Geldart, Baeyens, Pope, & Van De Wijer, 1981; Joseph et al., 2007; Sun & Grace, 1992). Chew & Hrenya (2011), Chew, Wolz, & Hrenya (2010) and Dahl & Hrenya (2005) have used a wide range of continuous-size distributions including Geldart group B and D. They have shown that the average particle diameter decreases along the bed height, and segregation increases by increasing the width of the particle size distribution. The Gaussian and log-normal mixtures with less than 10% standard deviation to average diameter ratio (σ/d_{ave}) have negligible segregation and because of experimental limitations they were considered as monodisperse (Chew et al., 2011). Moreover, the difference between minimum-to-maximum diameter in their system is wide (180–800 μm) and the effect of the type of size distribution

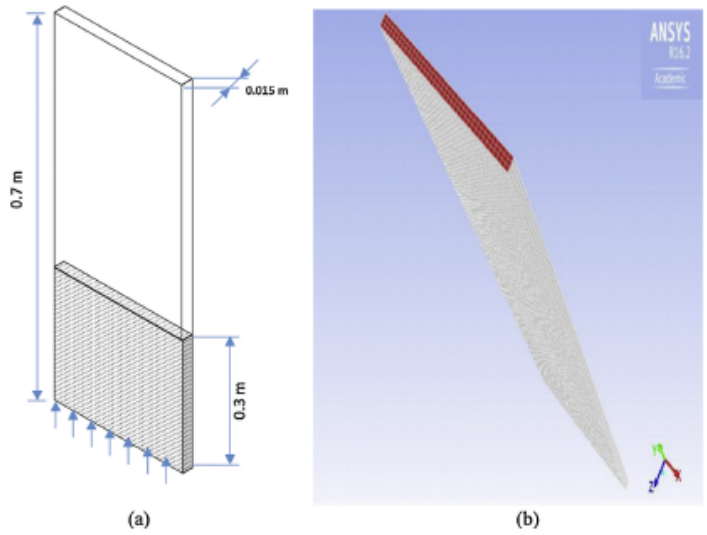

Fig. 1. (a) Geometric dimensions of the pseudo-2D physical bed and (b) 3D meshed computational bed.

Table 1
Simulation parameter settings.

Quantity	Value
Column dimensions (m)	$0.3 \times 0.7 \times 0.015$
Static bed height (m)	0.3
Gas density (kg/m^3)	1.225
Gas viscosity (kg/m s)	1.7894×10^{-5}
Particle diameter (μm)	400–600
Particle density (kg/m^3)	2500
Particle–particle coefficient of restitution	0.9
Specularity factor	0.0001–0.5
Number of parcel	1,000,000
Number of particle per parcel	10–24
Packing limit	0.63

on the narrow range of Geldart group B particles (400–600 μm) is overlooked but was investigated in our study. There are few studies reported in the literature on the use of CPFD and DDPM models to simulate circulating fluidized beds with polydispersed particles (Fotovat et al., 2015; Wang et al., 2015). However, more information is needed on the segregation and mixing characteristics of polydispersed particles using these hybrid E–L approaches.

In our study, a DDPM-based CFD model was developed on the ANSYS FLUENT software platform to analyze the hydrodynamics in a bubbling fluidized bed. Simulations were performed in a pseudo-2D bubbling fluidized bed configuration using the DDPM model and validated by experimental data for size and pattern of bubble flow, and the velocity and circulation patterns of particles reported in literature. The effects of wall friction on the pseudo-2D bubbling fluidized bed on the prediction accuracy were analyzed. The model was further used to study the effects of particle-size distribution on the segregation behavior of the pseudo-2D fluidized bed, using the Rosin–Rammler distribution scheme in a narrow range of particle diameters.

Modeling approach and simulation setup

Governing equations

The mass conservation equation for the gas phase is given by

$$\frac{\partial\left(\varepsilon_g\rho_g\right)}{\partial t}+\nabla\cdot\left(\varepsilon_g\rho_g\vec{v}_g\right)=0, \tag{1}$$

and the momentum conservation for the gas phase is determined by

$$\frac{\partial\left(\varepsilon_g\rho_g\vec{v}_g\right)}{\partial t}+\nabla\cdot\left(\rho_g\vec{v}_g\vec{v}_g\right)=-\varepsilon_g\nabla p_g+\nabla\cdot\tau_g+\varepsilon_g\rho_g\vec{g}$$
$$+K_{\mathrm{DPM}}\left(\vec{v}_{\mathrm{DPM}}-\vec{v}_g\right)+S_{\mathrm{DPM,explicit}} \tag{2}$$

where, ε_g denotes the volume fraction of gas phase, ρ_g density of gas phase, $\vec{v}_g$ gas phase velocity, p_g pressure of gas phase, τ_g shear tensor of the gas phase, K_{DPM} coefficient of drag taken from the granular phase, obtained using the Gidaspow drag model for calculations (Ding & Gidaspow, 1990), $\vec{v}_{\mathrm{DPM}}$ particle-averaged velocity of the considered discrete phase, and $S_{\mathrm{DPM,explicit}}$ an optional mass and momentum source term.

The equation of particle motion that is solved to determine the particle velocity and position in the gas phase is given by

$$\frac{d\vec{v}_p}{dt}=F_D\left(\vec{v}_g-\vec{v}_p\right)+\frac{\vec{g}\left(\rho_p-\rho_g\right)}{\rho_p}+\vec{F}_{\mathrm{interaction}}, \tag{3}$$

where, $\vec{v}_p$ denotes the particle velocity, $\vec{v}_g$ gas velocity, and F_D drag between gas and particles calculated using

$$F_D=\frac{18\,\mu C_d Re}{24\rho_p d_p^2}, \tag{4}$$

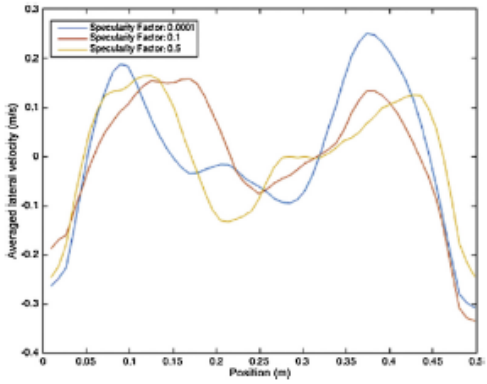

Fig. 2. Averaged vertical velocity at height of 0.25 m above the distributor using one cell in the thickness dimension for differing specularity factors.

where, C_d is the coefficient of drag calculated using the same drag model used in giving K_{DPM}. The particle–particle interaction is estimated from the granular phase stress tensor using

$$F_{\text{interaction}} = -\frac{1}{\rho_p}\nabla \cdot \tau_p, \tag{5}$$

where, τ_p denotes the solid stress including solid pressure, normal stress, and shear stress:

$$\tau_p = -p_p I + \varepsilon_p \mu_p \left(\nabla \vec{v}_p + \nabla \vec{v}_p^{\,T}\right) + \varepsilon_p \left(\lambda_p - \frac{2}{3}\mu_p\right) \nabla \cdot \vec{v}_p I, \tag{6}$$

Here the solid pressure p_p is defined as

$$p_p = \varepsilon_p \rho_p \Theta + 2\rho_p (1 + e_{ss}) \varepsilon_p^2 g_0 \Theta \tag{7}$$

where, g_0 is a correction factor representing the radial distribution function that modifies the probability of collisions between grains in dense areas, and Θ the granular temperature representing the kinetic energy of the fluctuating particles derived from kinetic theory model as

$$\frac{3}{2}\left[\frac{\partial\left(\varepsilon_p \rho_p \Theta\right)}{\partial t} + \nabla \cdot \left(\rho_p \vec{v}_p \vec{v}_p \Theta\right)\right] = \tau_p : \nabla \vec{v}_p + \nabla \cdot \left(k_\Theta \nabla \Theta\right) - \gamma_\Theta + \phi_{pg}, \tag{8}$$

where, the right-hand side terms represent the generation of energy via the solid stress tensor, the diffusion of energy, the collisional dissipation of energy, and the energy exchange between the gas and solid phases. The left-hand side terms represent convection and diffusion. Eq. (8) was solved algebraically by neglecting the convection and diffusion terms in the transport equation (Syamlal, Rogers, and O'Brien, 1993). Algebraic granular temperature conservation and modeling of the solid pressure have been proven to be acceptable for dense bubbling systems for which the local generation and dissipation of granular energy strongly outweighs the convective and diffusive fluxes crossing the cell boundaries (Boemer, Qi, Renz, Vasquez, & Boysan, 1995; Cloete et al., 2012; Van Wachem, Schouten, Van den Bleek, Krishna, & Sinclair, 2001).

System description

The simulation setup was configured based on two sets of widely used experimental data reported in the literature (Hernández-Jiménez et al., 2011; Laverman, Roghair, Annaland, & Kuipers, 2008). The first set of experimental data were collected on a pseudo-2D fluidized bed of dimensions 0.5 m (width) × 1 m (height) × 0.005 m (thickness). The particles of the bed material are made of ballotini glass of density 2500 kg/m^3 and average diameter 700 μm. The superficial gas velocity was 0.62 m/s, the minimum fluidization velocity was 0.35 m/s, and the static bed height was 0.3 m. This setup was used to evaluate the DDPM in predicting the effect of wall friction using one cell in the thickness direction. A second set of experimental data was collected on a pseudo-2D fluidized bed with dimensions of 0.3 m (width) × 0.7 m (height) × 0.015 m (thickness). Bed materials were glass beads of Geldart-B with a narrow diameter distribution of 400–600 μm (Laverman et al., 2008). An average particle diameter of 485 μm was used for single diameter simulations (Li, Grace, & Bi, 2010). The fluidization agent of air was passed through a porous distributor plate at a minimum fluidization velocity (U_{mf}) of 0.18 m/s reported by Laverman et al. (2008). The static bed height is 0.3 m. The superficial gas velocity was kept constant at 0.45 m/s around 2.5 U_{mf} to stay within the bubbling regime. The time-averaged vertical velocity of particles and the averaged solid volume fraction are calculated using

$$V_{py}(x,y,z) = \sum_{t=1}^{N} C_t(x,y,z) V_{py,t}(x,y,z) / \sum_{t=1}^{N} C_t(x,y,z), \tag{9}$$

$$\varepsilon_p(x,y,z) = \sum_{t=1}^{N} \varepsilon_{p,t}(x,y,z)/N, \tag{10}$$

where, N is the number of snapshots, and C_t is an indicator (0 inside the bubble and 1 in the emulsion phase) defined by a threshold that distinguishes bubbles from the dense phase, the recommended value being the arithmetic mean between the maximum and minimum solid volume fraction (Hernández-Jiménez et al., 2011). Therefore, if the solid volume fraction of a cell is less than the threshold value of 0.3, the cell is considered a bubble with $C_t = 0$; otherwise, dense phase with $C_t = 1$. As bubbles are a part of the bed that are assumed to be free of solids, the influence of particles inside the bubbles on the particle velocities in the emulsion phase is corrected by removing the velocity of the particles in the bubbles. ImageJ was used to determine the surface area and mass centers of the bubbles; the equivalent bubble diameter was calculated using (Hernández-Jiménez et al., 2011; Laverman et al., 2008; Li et al., 2010)

$$d_b = \sqrt{\frac{4S}{\pi}} \tag{11}$$

Initially, the contours of the solid volume fraction were adjusted using a color threshold and then the binary figures were created; bubbles were then detected, and their area was calculated as determined from the number of pixels reported for each bubble. Then the equivalent bubble diameters were averaged for 10 s from 20 to 30 s of simulation at frequency rate of 10 frames per second.

Computational geometry

A 3D computational column was generated to study the hydrodynamic properties of the bubbling fluidized bed. The movement of particles in the third dimension (bed thickness) and their collisions with the back and front wall perpendicular to the third dimension is only observed in a 3D setting. The column includes two parts: the bed and the freeboard, which are divided by an interface boundary condition (Fig. 1).

The particles are initially injected into the bed zone using the interface technique, which employs two overlapping interface boundary conditions to connect two fluid zones. The bed houses the initial injection of particles with a solid volume fraction of 0.60. The 3D system was uniformly meshed using the structured hexahedral cells with edge sizes of 5 mm in the height and width

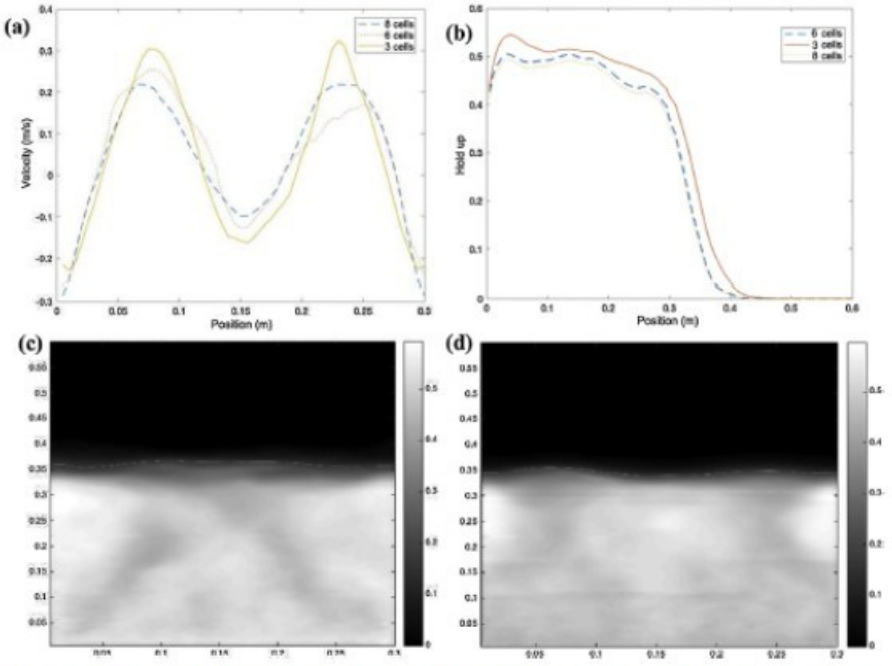

Fig. 3. (a) Time-averaged vertical velocity profiles at 10 cm above the bed, (b) solid holdups along the bed height obtained for differing numbers of computational cells in the thickness direction, (c) time-averaged solid volume fraction obtained using three cells, (d) time-averaged solid volume fraction obtained using six cells.

directions, respectively. Initially, one cell along the thickness of the column was used to study the effect of wall friction, using a thinner geometry (5 mm bed thickness) reported in the literature (Hernández-Jiménez et al., 2015). Then, the third dimension was discretized into 3, 6, and 8 computational cells along the thickness of the column, giving grid sizes of 5, 2.5, and 1.875 mm in a bed 15 mm thick (Laverman et al., 2008).

Boundary conditions and solver setup

A boundary condition at the bottom of the bed was paired with a uniform gas velocity to represent a porous gas distributor. A reflection boundary condition was used to prevent the DDPM tracking particles from draining out of the system. An atmospheric pressure outlet was considered as gas exit that allows the particles to escape out of the system as well. No-slip boundary condition was selected for the gas phase on the bed wall. The Johnson–Jackson boundary condition was used to calculate the granular phase shear force at the wall boundaries

$$\vec{\tau}_s = -\frac{\pi}{6}\sqrt{3}\phi\frac{\alpha_s}{\alpha_{s,\max}}\rho_s g_0 \sqrt{\Theta_s}\,\vec{U}_{s,\parallel}, \tag{12}$$

where, $\vec{U}_{s,\parallel}$ is the particle slip velocity parallel to the wall, $\alpha_{s,\max}$ volume fraction of particles at maximum packing, and ϕ specularity factor (SF), which determines the elasticity of the particle–wall interaction ranging from 0 for perfect specular collisions to 1 for perfectly diffuse collisions depending on wall roughness. Moreover, the coefficient of restitution between particle and wall in the Lagrangian frame is defined as ratio

$$e_{n,t} = \frac{V_{2,(n,t)}}{V_{1,(n,t)}}, \tag{13}$$

where, $V_{2,(n,t)}$ and $V_{1,(n,t)}$ are the particle velocities normal and tangential to the wall before and after collision, respectively. In this work, the node-based average particle variable was used to distribute the parcel's effects on neighboring mesh nodes (interpolation) (Adamczyk et al., 2014a; Patankar & Joseph, 2001) and to improve the grid dependency. By default, ANSYS Fluent maps the parcel's effects into the center of the computational cell, which is numerically unstable (Adamczyk et al., 2015). To average a variable φ on a mesh node (Coffield & Shepherd, 1987), we use

$$\bar{\varphi}_{\text{node}} = \sum_k N_{\text{in parcel}} w\left(\vec{x}_p^k - \vec{x}_{\text{node}}\right)\varphi_p, \tag{14}$$

where, φ_p is the particle variable, $N_{\text{in parcel}}$ the number of particles in the parcel, and $\bar{\varphi}_{\text{node}}$ the accumulation of the particle variable on the node for all parcels k, and $w\left(\vec{x}_p^k - \vec{x}_{\text{node}}\right)$ the weighting function or kernel. In this method, convergence characteristics are not tied to the Eulerian grid but add statistical errors to the solution (Garg, Narayanan, & Subramaniam, 2009). However, by regulating the kernel bandwidth, the user can balance the contribution from truncation and statistical errors (Garg, Narayanan, Lakehal, & Subramaniam, 2007). The Gaussian kernel was used as a weighting function with a Gaussian factor of 6 to store the particle vari-

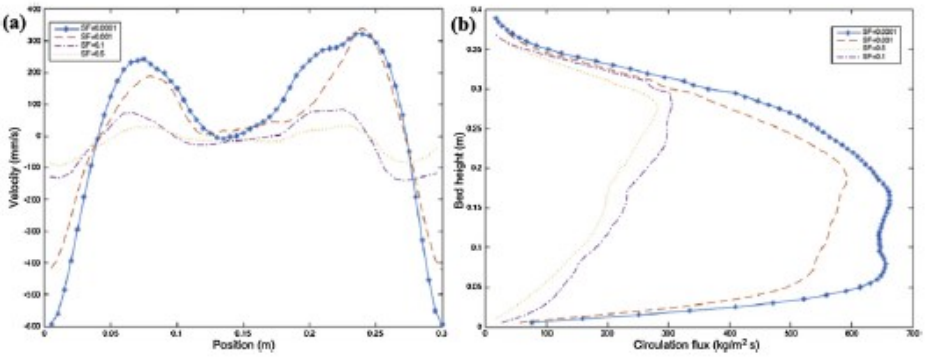

Fig. 4. (a) Time-averaged vertical velocity of solids in the emulsion phase at 105 mm above the bed. (b) Rate of circulation of particles averaged over time and width direction (simulation time: 30 s).

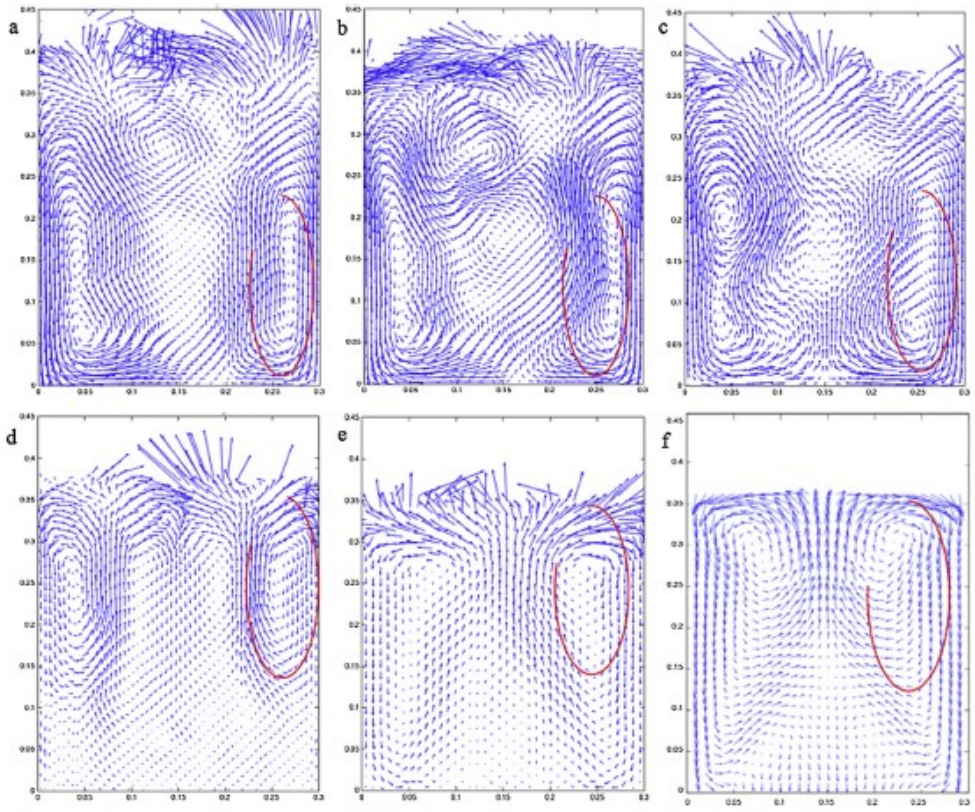

Fig. 5. Time-averaged velocity vectors of dense phase predicted for differing specularity factors (SFs): (a) 0.0001, (b) 0.001, (c) 0.005, (d) 0.1, and (e) 0.5, compared with (f) experimental results (Laverman et al., 2008).

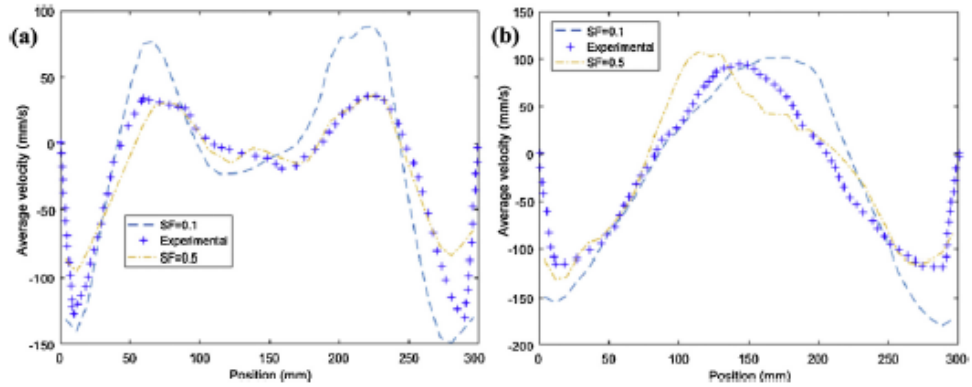

Fig. 6. Time-averaged vertical velocity of solids in emulsion phase at (a) 105 mm and (b) 245 mm above the bed (simulation time: 30 s).

able on the mesh nodes and redistribute them back to the cells (Apte, Mahesh, & Lundgren, 2008; Kaufmann, Moreau, Simonin, & Helie, 2008). A constant kernel bandwidth leads notably to a constant statistical error with grid refinement (Garg et al., 2009; Subramaniam, 2013). Further investigation on the time-dependent kernel width is outside the scope of this study. The phase-coupled SIMPLE scheme was used for pressure–velocity coupling. A second-order upwind scheme was used for the momentum equation and the QUICK method for the spatial discretization of volume fraction. The first-order implicit transient formulation was used for temporal discretization. Table 1 lists those parameters used in the simulations. All of the simulations were performed for 30 s with the same time step of 1×10^{-5} s for both particle and fluid calculations. Given the frequency rate of 1000 frames per second, the last 25 s of each simulation was used for averaging properties.

Results and discussion

The micro-to-macro scale hydrodynamic properties of the fluid bed that were studied include solid vertical velocity, velocity vectors, size of the bubbles, solid volume fraction, mixing, segregation, and probable location of particles with differing diameters.

Effect of grid size in the thickness direction on wall friction

In the literature, a mesh-independent behavior of the dense discrete phase model was reported when simulating fluidized beds with squared cells with height and width of 10 particle diameters (Cloete, Johansen, Braun, Popoff, & Amini, 2010). A uniform mesh of the same dimensions was chosen for the height and width directions to achieve a good resolution in solid flow. Moreover, a mesh-dependence study was performed to evaluate the effect of the number of computational cells in the thickness direction on prediction accuracy. Originally, a bed 0.5 m in width × 1 m in height × 0.005 m in thickness was used in the experiments conducted by Hernández-Jiménez et al. (2011) and meshed with one computational cell in the thickness dimension (5 mm). Height and width directions were discretized using (5 mm) squared grids (10 times the diameter of a particle). The variation in SF did not significantly affect the velocity of the particles when using one computational cell in the thickness dimension (Fig. 2).

The use of just one computational cell in the thickness of the thin bubbling fluidized bed ignores the gas velocity variations in the thickness direction although the particles can still be tracked in a Lagrangian frame and the solid flow is still three dimensional. However, we note that in using the hybrid E–L method, the interactions among particles depend on the Eulerian frame. Therefore, the effect of front and back wall friction of the pseudo-2D bed on the solid flow is observed only if we have a sufficient number of cells in the thickness dimension. Using one cell in the thickness direction is the reason why Liang et al. (2014) were unable to capture the effect of wall friction.

Moreover, as particles rebounds off the wall in a Lagrangian frame, the change in particle momentum is determined by the normal and tangential coefficient of restitutions. The same results were observed by changing the coefficient of restitution and no wall friction effect was observed. This can be explained by the fact that the velocity in the bed thickness direction is very small, and the effect of the coefficient of restitution on the interactions with the front and back walls is negligible; it does not have any effect on the velocity in the x and y (bed height and width) directions. Because the coefficient of restitution from the Lagrangian frame does not reproduce the wall friction in this instance, a SF with a greater number of cells in the thickness direction was used. Therefore, the thickness dimension of a pseudo-2D fluidized bed was discretized into more than one computational cell to observe the effect of wall friction on the solid flow. A fluidized bed of 0.5 m (width) × 1 m (height) × 0.005 m (thickness) used for the above simulation was too thin for discretization. It led to a computational divergence because of a large computational-cell aspect ratio if the thickness is discretized into more than one computational cell. Therefore, the pseudo-2D fluidized bed of dimensions 0.3 m (width) × 0.7 m (height) × 0.015 m (thickness) as used in the experiments conducted by Laverman et al. (2008) was chosen for the rest of the simulations in this study. Fig. 3 shows the results for three different numbers of cells in the thickness direction. In Fig. 3(a) and (b), increasing the number of computational cells in the thickness direction from three to eight did not change the vertical velocity of particles at 10 cm above the bed. However, the solid holdup decreased with increasing number of cells in the thickness direction but the change was not significant when the number of cells increased from six to eight. Fig. 3(c) and (d) shows the time-averaged solid volume fraction and the bed surface predicted using 3 and 6 cells in the thickness direction, respectively. The simulation bed height was extracted from the time-averaged solid volume fraction with a threshold of 10%. The experimental bed height was extracted from the position of the last upward velocity vector on top of the bed surface,

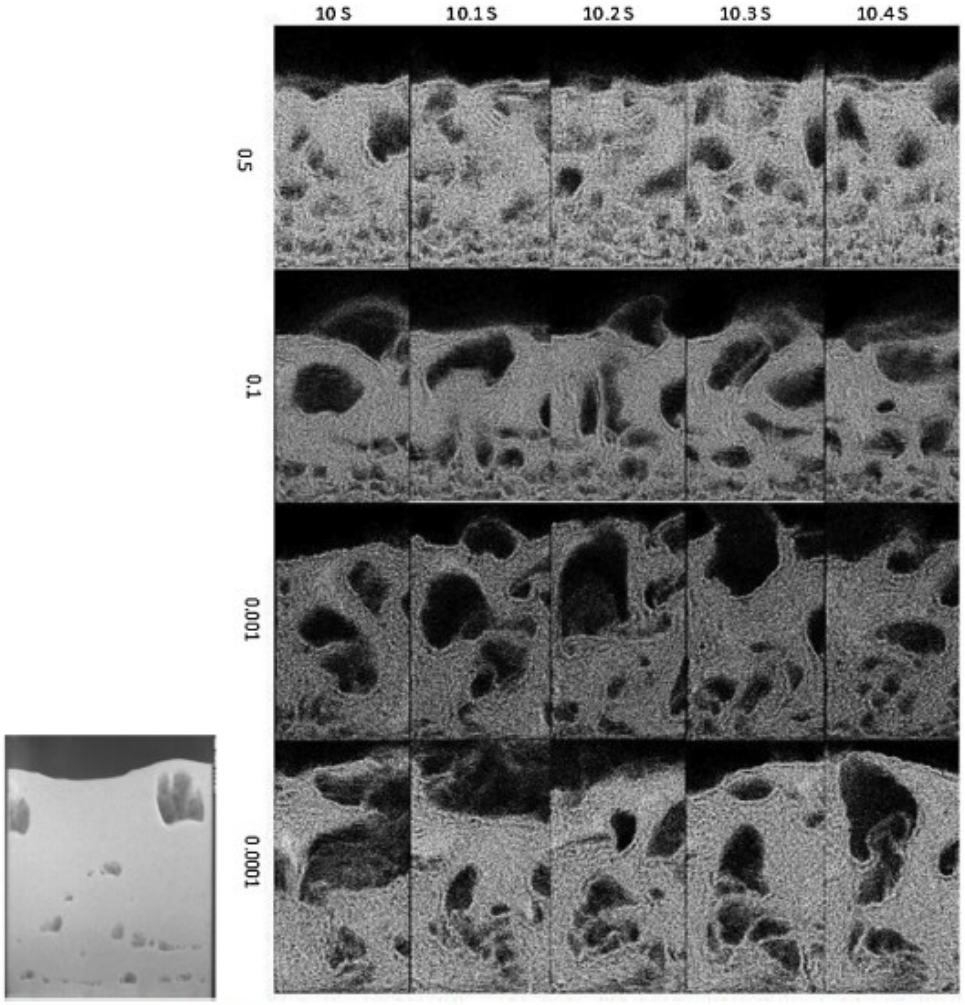

Fig. 7. Instantaneous snapshot of the predicted bubbling bed at differing specularity factors (right) and experimental data at superficial gas velocity of 0.45 m/s (Laverman et al., 2008) (left).

which was estimated to be 0.350 m (Laverman et al., 2008). The bed heights predicted by the CFD simulations were 0.375, 0.352, and 0.351 m using 3, 6, and 8 cells, respectively, in the thickness direction. Although, the use of three cells in the thickness direction could well predict the velocity of particles, it over-predicted the expanded bed height. Other studies showed that the bed height was a more reliable parameter for the mesh-independence study (Cloete et al., 2013). This study showed that the use of six cells in the thickness dimension predicts both particle velocities and bed expansion well.

Fig. 4(a) shows the time-averaged particle velocity at a location of 105 mm above the distributor. Increasing SF from 0.001 to 0.1 decreases significantly the downward velocity of the particles beside the wall, thereby confirming the circulation pattern as presented by velocity vectors (see next section). To gain a better understanding of the wall-friction effect, the rate of circulation which is the vertical solid flux was calculated, and averaged over cross sections of the bed along the bed height and time (Altantzis et al., 2015; Sánchez-Delgado et al., 2013),

$$Q = \frac{1}{A_c} \int_{x_{min}}^{x_{max}} \int_{z_{min}}^{z_{max}} \rho_p \varepsilon_p \left| \vec{v}_n \right| dxdz, \tag{15}$$

where, A_c is the cross section are of the bed, and $\left|\vec{v}_n\right|$ the vertical component of the solid velocity in both upward and downward directions. From Fig. 4(b), the rate of circulation decreases rapidly at bed heights below 25 cm by increasing the SFs; however, the change in SF does not affect the rate of the circulation of particles close to the top of the bed and the location at bed heights above 25 cm because of the presence of large bubbles and vigorous mixing

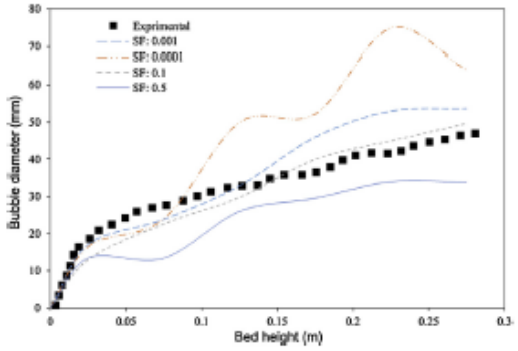

Fig. 8. Mean bubble diameter as a function of height from the distributor for differing specularity factors compared with experiments (Laverman et al., 2008).

at the top of the bed. Note that SF effects are more profound at the bottom of the bed where large bubbles are not formed. The bubbles grow at a high rate at the bottom of the bed with low SF and subsequently leads to vigorous mixing and higher velocities of particles. The higher rate of expansion of bubbles affects the solid flow by formation of wakes at the bottom of the growing bubbles.

Validation of solid velocity and circulation pattern

The velocity vectors were compared with those obtained from experimental data reported in the literature to evaluate the accuracy in predicting the circulation patterns of the solid particle flow in the model. From Fig. 5, the change in SF affects the pattern of the flow. An increasing SF leads to a shift in the vortex center toward the surface of the bed and further away from distributor plate, which is in agreement with the experimental results (Laverman et al., 2008). At small SFs, the downward circulation of the particles, especially beside the walls and at the bottom of the system, is profound and a vigorous mixing occurs in the whole bed. This is shifted to the top of the bed by increasing SF from 0.005 to 0.1. The recirculation centers are formed through bubble movements. That means that increasing SF would inhibit bubble formation at the bottom of the bed because of a higher pressure at the bottom of the reactor. Moreover, the bed height decreases and the bed becomes more packed if SF is increased. Increasing SF increases wall friction, which decreases the expansion of the emulsion phase (dense phase). Fig. 6 compares the averaged vertical velocity of the solid phase in the emulsion phase with experimental data at two different bed heights and higher SFs. There is an acceptable agreement between the results and experimental data, although the under-prediction of the particle velocity beside the wall at $SF = 0.5$ and the over-prediction of the results at $SF = 0.1$ may be due to the simplistic assumption of the particle collision model used in the DDPM model.

Bubble dynamics

Fig. 7 shows snapshots of particles in the bubbling condition simulated at different SFs; Fig. 8 presents the bubble diameter as a function of bed height for different SFs. Increasing SF reduces the size of bubbles and its effect is more significant at the top of the bed where coalescence happens. Large bubbles are formed using a low SF that corresponds to low wall friction, and solid flow is near the slugging regime. As there is little resistance to bubble grows, the bubble grows quickly and coalesces in consequence of the strong wake forming under the bubble. The downward flux of particles beside the wall due to gravity has an exponential increase when decreasing SF and helps the bubble grow at the center of the bed. Increasing SF leads to an increase in the number of small bubbles distributed at the bottom of the bed. However, the bubbles cannot grow significantly as the particles exert more friction on bubbles. The movement of particles is suppressed because momentum is dissipated in the walls. Therefore, drag is unable to move the particles and the gas is forced to pass through the bed as small bubbles. Consequently, drag is distributed over the entire bed compared with low SF conditions where drag is mostly present at the center of the bed. Moreover, there is a higher particle fraction inside

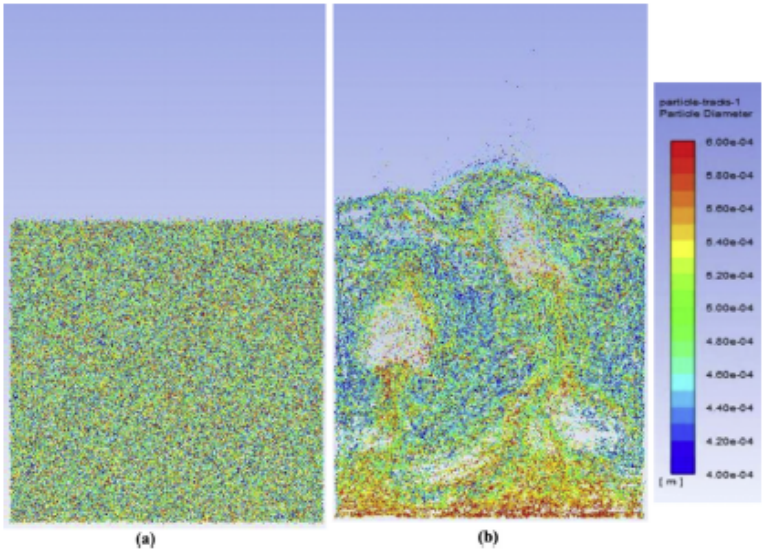

Fig. 9. Snapshots of particles at (a) well-mixed initial conditions and (b) after 30 s.

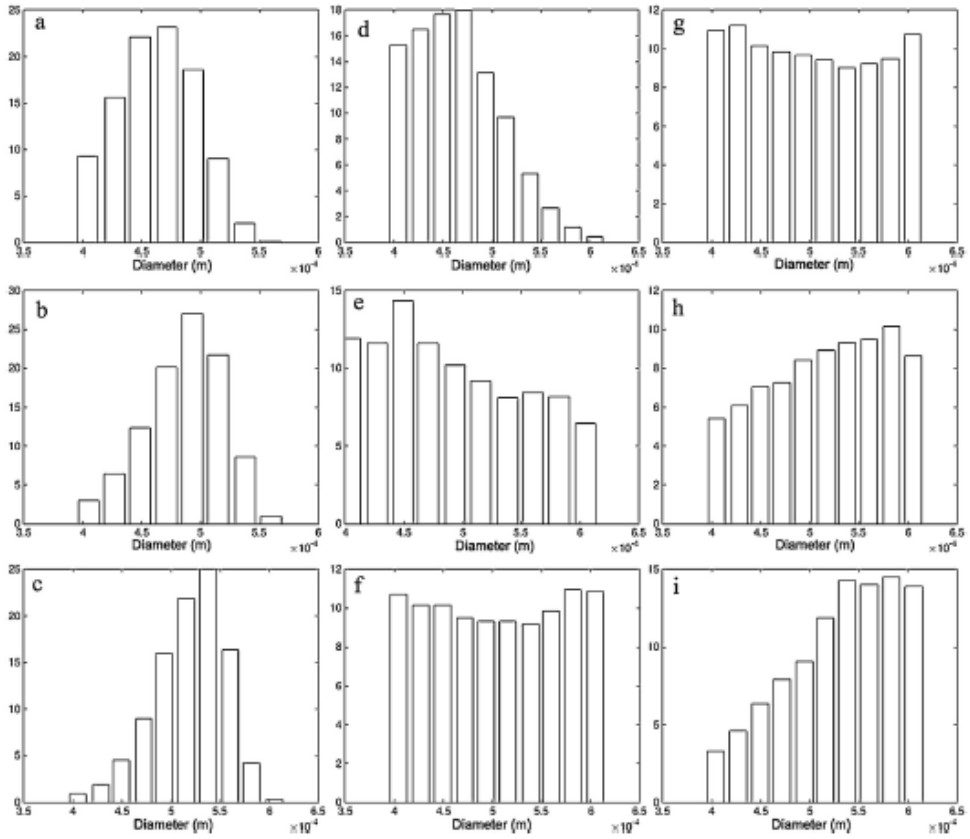

Fig. 10. Histograms of particle size distributions (before mixing); each injection is divided into 10 different particle diameters.

Table 2
Injected particle properties and time-averaged mixed particle properties at bed positions.

Case	De Brouckere diameter (μm)	Mean diameter (μm)	Rosin–Rammler spread parameter	STD of the diameter of the particles before mixing (σ_{IP})	Number of particles	STD of the averaged particle diameter of the cells (σ_{MP})	Mixing index (%)
a	458	451	15	33.3	1.524×10^7	9.377	71.84
b	481	474	15	33.6	1.302×10^7	11.386	66.11
c	514	499	15	36.9	1.135×10^7	17.019	53.88
d	460	448	6.5	44.4	1.569×10^7	10.922	75.40
e	494	470	3.5	65.2	1.332×10^7	26.404	59.50
f	490	467	1.5	65.5	1.361×10^7	30.794	52.99
g	497	470	1.5	65.2	1.332×10^7	33.4808	48.65
h	488	461	3.5	61.8	1.423×10^7	32.514	47.39
i	527	490	6.5	56.3	1.180×10^7	31.8755	43.38

the bubbles because less separation occurs between solid and gas phase if SF is high.

Effect of continuous particle size distribution

A perfectly mixed reactor is one in which the probability of finding a particle of a certain diameter is the same for all points in the bed. However, in fluidized bed reactors, perfect mixing does not happen in practice. In Fig. 9(a) and (b), particles are injected into the system initially in a well-mixed condition and particle segregation then takes place during fluidization. Although large particles are dispersed in the bed, a considerable portion of the large particles accumulate at the bottom of the bed. As indicated, large particles are dragged toward the top of the bed following the bubble pathway. The cloud and wake area of the bubbles are mostly formed by larger particles. This can lead to different mass and heat transfer rates between the bubbles and emulsion phase for different particle size distributions.

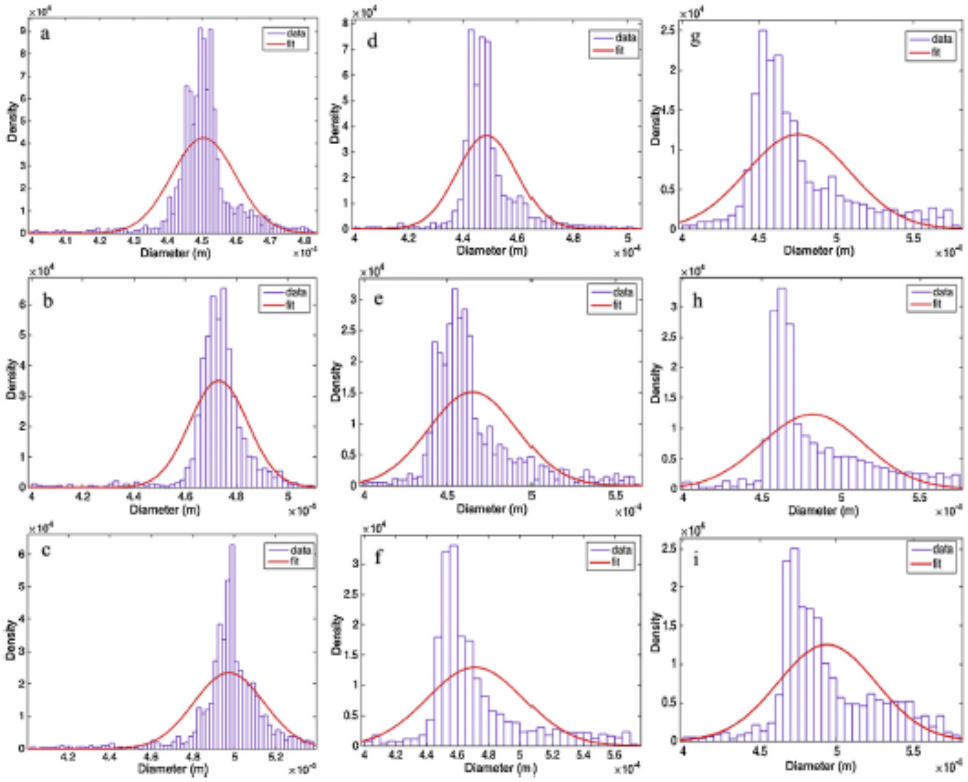

Fig. 11. Time-averaged particle diameter of the cells (histograms) and fitted normal distribution curves.

To study the distributional effect of particle size on mixing and segregation in a bubbling fluidized bed, nine different continuous distributions for particle size were analyzed including narrow, wide, and flat distributions (Fig. 10). As mentioned earlier, most of the previous experimental studies were conducted with binaries or a wide range of particle sizes; narrow particle-size distributions were also considered as monodispersed because of experimental sieving limitations (Chew et al., 2011). Therefore, the effect of purely different distributions with less than 10% change in mean diameter of particles and less than 10% standard deviation-to-mean diameter ratio were considered. Cases a–c are close to normal Gaussian distributions, whereas Cases d and i are close to log-normal distributions with different average diameters, and Cases e–g, and h are close to flat distributions. The average diameter and standard deviation of particle sizes are presented in Table 2. Note that the difference between the minimum and maximum average diameter is less than 50 μm, which is around 10% of the average diameter. The Rosin–Rammler spread values of 15 and 6.5 create the Gaussian and log-normal distributions whereas values of 3.5 and 1.5 give flat distributions.

For each simulation, particles totaling a mass of 1.9 kg with a certain distribution were injected into 1 million parcels at the first time-step. The superficial velocity was kept constant at 0.45 m/s for all cases with $SF = 0.5$ to consider the wall friction. All fluidization simulations were performed for 30 s and the average diameter of particles in each cell was calculated over the last 20 s of simulations. This average particle diameter represents the probability of the presence of a particle with a certain diameter at the given local point of the bed. Fig. 11 shows the histogram of this time-averaged particle diameter of the cells along with a fitted Gaussian normal distribution curve. If the particles were perfectly dispersed over the bed, these histograms would be very narrow whereas segregation would result in wide histograms with larger standard deviations. Local size distributions have been reported to mimic the overall size distribution of particles in most regions of the bed (Dahl & Hrenya, 2005). Cases a–c with Gaussian distributions each have a local Gaussian distribution shape with a narrow standard deviation from the average size; good mixing is observed in these cases and confirms an insignificant effect with extreme-sized particles in small proportions. Cases d and i with log-normal distribution show a mean diameter effect of extreme-sized particles in large proportions that flattens the distribution curve for larger mean diameter and consequently results in more segregation. As expected, a flat size distribution results in wide local size distribution.

To quantify the dispersion within a mixture of a certain particle-size distribution in the fluidized bed, a mixing index that is defined,

$$Mixing\ Index = \frac{\sigma_{IP} - \sigma_{MP}}{\sigma_{IP}} * 100, \tag{16}$$

where, σ_{IP} is the standard deviation of the diameter of the injected particles (before mixing), and σ_{MP} is the standard deviation of the time-averaged particle diameter of the cells (local).

A mixing index of 100% means that all particles are found at all positions with the same probability; a mixing index of zero means complete segregation or in other words the same standard devi-

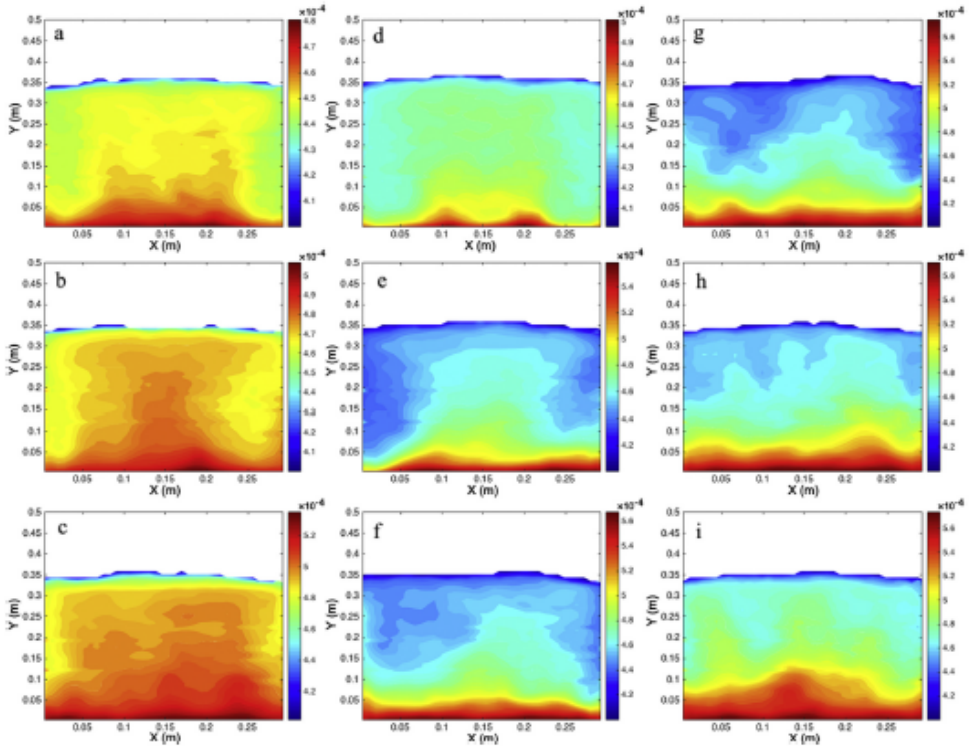

Fig. 12. Time-averaged particle diameter of the cells in the bed for differing particle-size distributions.

ation remains the same as before mixing. Including the standard deviation of particle size before mixing helps in determining the role of fluidization in mixing. Table 2 lists all case studies with mixing index ranging from 43.38% to 75.40%. Increasing the mean particle diameter in Gaussian distribution samples decreased the standard deviation of averaged cell diameter and consequently increased the mixing index. Comparing Cases c and e shows that a smaller standard deviation after mixing does not guarantee a higher mixing index. A higher mixing index indicates better mixing by means of bubbling fluidization in Case e even though it has a larger standard deviation. If we leave the system in minimum fluidization without any mixing, the mixing index of the sample with smaller standard deviation (before mixing) is always higher because of segregation due to drag and gravity. As is evident, Case d, which has a log-normal distribution with large proportions of small particles, has the highest mixing index and thus shows the dominant role of the mean diameter even in narrow distributions. The samples with flat distributions produce the lowest values for the mixing index and the larger standard deviations, thereby confirming their similar segregation behavior with binary mixtures. In general, increasing the mean diameter decreases the mixing index in a constant size distribution but a change in shape of the size distribution from a Gaussian to a flat distribution may have more effect than changing the mean particle diameter.

To gain a better understanding of the probable location of different particles in the bed, contours of the time-averaged local particle diameter in bed area are presented (Fig. 12). The large particles are present at the bottom and center of the bed whereas the small particles are located beside the wall and close to the surface of the bed. Increasing the mean particle size in the Gaussian distribution cases results in a low accumulation of small particles beside the wall, whereas a larger jetsam layer of large particles forms at the bottom of the system. Comparing Cases d and i with log-normal and mirror log-normal distributions shows the effect of extreme sized particles in large proportions in segregations and jetsam formations. Case d with a large proportion of small particles has a thin layer of jetsam whereas Case i with a large proportion of coarser particles has a thick layer of jetsam and minimum mixing arising from bubbling, in agreement with the results of Chew and Hrenya (2011) on forming a bubble-less layer despite the bed being fully fluidized. Changing shape of the size distribution to a flat distribution increases the chance of jetsam formation and segregation even at mixtures with the same mean diameter. The best mixing was achieved in Case d, which has particles with a mean diameter of 448 μm and a large proportion of small particles with a log-normal distribution before mixing. This confirms the advantage of using log-normal distributions containing a small proportion of large particles (Chew et al., 2010). This can be explained by the fact that the decrease of the particle size increased the ratio of drag-to-collisional force among particles. Decreasing the collision force among the particles causes smooth shifts in the solid phase that decreases the mixing time and consequently provides better mixing. Therefore, fluidization is controlled by smaller particles with a thin layer of jetsam at the bottom of the bed. Note that a higher concentration of larger particles at the center of the bed was related to bubble pathways at the center of the bed that could carry them toward the top of the bed. Increasing the mean particle-size distribution causes the formation of a thick layer of jetsam at the bottom of the bed that decreased

the size and formation of the bubbles. Suppressing the formation of bubbles, which are a major mixing agent in the bed, decreases the mixing significantly. This was more pronounced when a flat distributor was used and a thick jetsam was formed at the bottom of the bed. As seen in Case i, this thick jetsam plays the role of a packed bed distributor, the rest of the bed being mixed uniformly.

Conclusions

A hybrid E–L model was developed with a 3D computational geometry to simulate the hydrodynamics of a thin bubbling fluidized bed. The time-averaged velocity vectors of the emulsion phase and the axial velocity of the single size particles were validated with good agreement with the experimental results obtained. Simulations showed that ignoring wall friction during simulations would affect both the velocity of particles and circulation pattern. The size and general pattern of the bubbles in the bed predicted at differing SF were compared with experimental results. A decrease in SF was shown to lead to a greater expansion in the system and the formation of large bubbles. The particle-size distribution is an advantage of the Lagrangian framework in the DDPM method and was considered in studying the mixing and segregation of particles. A new mixing index for continuous particle-size distributions was defined using the standard deviation of the particle size before mixing and the standard deviation of the local size distribution. The results indicate a local accumulation of large particles at the bottom and center of the bed. The mixing of particles with various diameters not only was improved by decreasing the mean diameter and the width of distribution, but the shape of the distribution had a considerable impact on mixing and segregation of particles. Although the polydisperse results need to be verified with experimental data, and the DDPM model cannot resolve the particle collisions as DEM does, it is a start in considering the particle-size distribution of narrow-size-distributed mixtures that are considered to be monodispersed. Finally, the accuracy of the model can be improved by increasing the resolution of particle collisions using sub-grid filter models.

Acknowledgements

We thank Dr. David Dayton at RTI International for his help and valuable comments. We acknowledge a contribution from North Carolina Agricultural and Technical State University, supported by funds partially provided by U.S. Department of Energy (Grant #: EE0003138) and U.S. National Scientific Foundation (Grant #: HRD-1242152). Mention of a trade name, proprietary products or company name is for presentation clarity and does not imply endorsement by the authors or the university.

References

Adamczyk, W. P., Klimanek, A., Białecki, R. A., Węcel, G., Kozołub, P., & Czakiert, T. (2014). Comparison of the standard Euler–Euler and hybrid Euler–Lagrange approaches for modeling particle transport in a pilot-scale circulating fluidized bed. *Particuology, 15*, 129–137.

Adamczyk, W. P., Kozołub, P., Klimanek, A., Białecki, R. A., Andrzejczyk, M., & Klajny, M. (2015). Numerical simulations of the industrial circulating fluidized bed boiler under air-and oxy-fuel combustion. *Applied Thermal Engineering, 87*, 127–136.

Adamczyk, W. P., Kozołub, P., Węcel, G., Klimanek, A., Białecki, R. A., & Czakiert, T. (2014). Modeling oxy-fuel combustion in a 3D circulating fluidized bed using the hybrid Euler–Lagrange approach. *Applied Thermal Engineering, 71*(1), 266–275.

Adamczyk, W. P., Węcel, G., Klajny, M., Kozołub, P., Klimanek, A., & Białecki, R. A. (2014). Modeling of particle transport and combustion phenomena in a large-scale circulating fluidized bed boiler using a hybrid Euler–Lagrange approach. *Particuology, 16*, 29–40.

Altantzis, C., Bates, R. B., & Ghoniem, A. F. (2015). 3D Eulerian modeling of thin rectangular gas–solid fluidized beds: Estimation of the specularity coefficient and its effects on bubbling dynamics and circulation times. *Powder Technology, 270*, 256–270.

Andrews, M. J., & O'Rourke, P. J. (1996). The multiphase particle-in-cell (MP-PIC) method for dense particulate flows. *International Journal of Multiphase Flow, 22*(2), 379–402.

Apte, S. V., Mahesh, K., & Lundgren, T. (2008). Accounting for finite-size effects in simulations of disperse particle-laden flows. *International Journal of Multiphase Flow, 34*(3), 260–271.

Arastoopour, H., Gidaspow, D., & Abbasi, E. (2017). Polydispersity and the population balance model. In *Computational transport phenomena of fluid-particle systems*. pp. 55–80. Cham: Springer International Publishing.

Beetstra, R., van der Hoef, M. A., & Kuipers, J. A. M. (2007). Numerical study of segregation using a new drag force correlation for polydisperse systems derived from lattice-Boltzmann simulations. *Chemical Engineering Science, 62*(1–2), 246–255.

Benyahia, S., & Galvin, J. E. (2010). Estimation of numerical errors related to some basic assumptions in discrete particle methods. *Industrial & Engineering Chemistry Research, 49*(21), 10588–10605.

Boemer, A., Qi, H., Renz, U., Vasquez, S., & Boysan, F. (1995). Eulerian computation of fluidized bed hydrodynamics–A comparison of physical models. *Proceedings of the 13th International Conference on Fluidized Bed Combustion, Vol. 2*, 775. Retrieved from. http:// scholar. google. com/ scholar?hl=en&btnG=Search&q=intitle:eulerian+computation+of+fluidized+bed+hydrodynamics+-+a+comparison+of+a+physical+models#0

Chew, J. W., Hays, R., Findlay, J. G., Karri, S. R., Knowlton, T. M., Cocco, R. A., et al. (2011). Species segregation of binary mixtures and a continuous size distribution of Group B particles in riser flow. *Chemical Engineering Science, 66*(20), 4595–4604.

Chew, J. W., & Hrenya, C. M. (2011). Link between bubbling and segregation patterns in gas-fluidized beds with continuous size distributions. *AIChE Journal, 57*(11), 3003–3011.

Chew, J. W., Wolz, J. R., & Hrenya, C. M. (2010). Axial segregation in bubbling gas-fluidized beds with Gaussian and lognormal distributions of Geldart Group B particles. *AIChE Journal, 56*(12), 3049–3061.

Cloete, S., Johansen, S., Braun, M., Popoff, B., & Amini, S. (2010). Evaluation of a lagrangian discrete phase modeling approach for resolving cluster formation in CFB risers. May, *International Conference on Multiphase Flow*.

Cloete, S., & Amini, S. (2016). The dense discrete phase model for simulation of bubbling fluidized beds: Validation and verification. May, *ICMF–2016– 9th International Conference on Multiphase Flow*.

Cloete, S., Johansen, S. T., & Amini, S. (2012). Performance evaluation of a complete Lagrangian KTGF approach for dilute granular flow modelling. *Powder Technology, 226*, 43–52.

Cloete, S., Johansen, S. T., Braun, M., Popoff, B., & Amini, S. (2011). Evaluation of a lagrangian discrete phase modeling approach for application to industrial scale bubbling fluidized beds. In *Proceedings of the 10th International Conference on Circulating Fluidized Beds and Fluidization Technology* May.

Cloete, S., Johansen, S. T., Zaabout, A., van Sint Annaland, M., Gallucci, F., & Amini, S. (2015). The effect of frictional pressure, geometry and wall friction on the modelling of a pseudo-2D bubbling fluidised bed reactor. *Powder Technology, 283*, 85–102.

Cloete, S., Zaabout, A., Johansen, S. T., van Sint Annaland, M., Gallucci, F., & Amini, S. (2013). The generality of the standard 2D TFM approach in predicting bubbling fluidized bed hydrodynamics. *Powder Technology, 235*, 735–746.

Coffield, D., & Shepherd, D. (1987). Tutorial guide to Unix sockets for network communications. *Computer Communications, 10*(1), 21–29.

Dahl, S. R., & Hrenya, C. M. (2005). Size segregation in gas–solid fluidized beds with continuous size distributions. *Chemical Engineering Science, 60*(23), 6658–6673.

Davidson, J. F., & Harrison, D. (1966). The behaviour of a continuously bubbling fluidised bed. *Chemical Engineering Science, 21*(9), 731–738.

Deen, N. G., Annaland, M. V. S., Van der Hoef, M. A., & Kuipers, J. A. M. (2007). Review of discrete particle modeling of fluidized beds. *Chemical Engineering Science, 62*(1–2), 28–44.

Di Renzo, A., Di Maio, F. P., Girimonte, R., & Formisani, B. (2008). DEM simulation of the mixing equilibrium in fluidized beds of two solids differing in density. *Powder Technology, 184*(2), 214–223.

Ding, J., & Gidaspow, D. (1990). A bubbling fluidization model using kinetic theory of granular flow. *AIChE Journal, 36*(4), 523–538.

Fan, L. T., & Wang, R. H. (1975). On mixing indices. *Powder Technology, 11*(1), 27–32.

Feng, Y. Q., Xu, B. H., Zhang, S. J., Yu, A. B., & Zulli, P. (2004). Discrete particle simulation of gas fluidization of particle mixtures. *AIChE Journal, 50*(8), 1713–1728.

Fotovat, F., Abbasi, A., Spiteri, R. J., de Lasa, H., & Chaouki, J. (2015). A CPFD model for a bubbly biomass–sand fluidized bed. *Powder Technology, 275*, 39–50.

Garg, R., Narayanan, C., Lakehal, D., & Subramaniam, S. (2007). Accurate numerical estimation of interphase momentum transfer in Lagrangian–Eulerian simulations of dispersed two-phase flows. *International Journal of Multiphase Flow, 33*(12), 1337–1364.

Garg, R., Narayanan, C., & Subramaniam, S. (2009). A numerically convergent Lagrangian–Eulerian simulation method for dispersed two-phase flows. *International Journal of Multiphase Flow, 35*(4), 376–388.

Gauthier, D., Zerguerras, S., & Flamant, G. (1999). Influence of the particle size distribution of powders on the velocities of minimum and complete fluidization. *Chemical Engineering Journal, 74*(3), 181–196.

Geldart, D. (1969). *Fluidization engineering: By D. Kunii and O. Levenspiel*. New York: John Wiley and Sons, Ltd., 1969. 534 pp.; 220 illus. PriceÉ 6.12. 0. *Powder Technology, 3*(1), 255–256.

Geldart, D. (1972). The effect of particle size and size distribution on the behaviour of gas-fluidised beds. *Powder Technology, 6*(4), 201–215.

Geldart, D., Baeyens, J., Pope, D. J., & Van De Wijer, P. (1981). Segregation in beds of large particles at high velocities. *Powder Technology, 30*(2), 195–205.
Grace, J. R., & Sun, G. (1991). Influence of particle size distribution on the performance of fluidized bed reactors. *The Canadian Journal of Chemical Engineering, 69*(5), 1126–1134.
Harris, S. E., & Crighton, D. G. (1994). Solitons, solitary waves, and voidage disturbances in gas-fluidized beds. *Journal of Fluid Mechanics, 266*, 243–276.
Hashemi Sohi, A., Eslami, A., Sheikhi, A., & Sotudeh-Gharebagh, R. (2012). Sequential-based process modeling of natural gas combustion in a fluidized bed reactor. *Energy & Fuels, 26*(4), 2058–2067.
Hashemisohi, A., Wang, L., & Shahbazi, A. (2019). Dense discrete phase model coupled with kinetic theory of granular flow to improve predictions of bubbling fluidized bed hydrodynamics. *KONA Powder and Particle Journal, 36*, 215–223.
Hernández-Jiménez, F., García-Gutiérrez, L. M., Soria-Verdugo, A., & Acosta-Iborra, A. (2015). Fully coupled TFM-DEM simulations to study the motion of fuel particles in a fluidized bed. *Chemical Engineering Science, 134*, 57–66.
Hernández-Jiménez, F., Sánchez-Delgado, S., Gómez-García, A., & Acosta-Iborra, A. (2011). Comparison between two-fluid model simulations and particle image analysis & velocimetry (PIV) results for a two-dimensional gas–solid fluidized bed. *Chemical Engineering Science, 66*(17), 3753–3772.
Hong, K., Gao, Y., Ullah, A., Xu, F., Xiong, Q., & Lorenzini, G. (2018). Multi-scale CFD modeling of gas–solid bubbling fluidization accounting for sub-grid information. *Advanced Powder Technology, 29*(3), 488–498.
Hoomans, B. P. B., Kuipers, J. A. M., Briels, W. J., & van Swaaij, W. P. M. (1996). Discrete particle simulation of bubble and slug formation in a two-dimensional gas-fluidised bed: A hard-sphere approach. *Chemical Engineering Science, 51*(1), 99–118.
Hoomans, B. P. B., Kuipers, J. A. M., & van Swaaij, W. P. M. (2000). Granular dynamics simulation of segregation phenomena in bubbling gas-fluidised beds. *Powder Technology, 109*(1-3), 41–48.
Huilin, L., Yunhua, Z., Ding, J., Gidaspow, D., & Wei, L. (2007). Investigation of mixing/segregation of mixture particles in gas–solid fluidized beds. *Chemical Engineering Science, 62*(1–2), 301–317.
Igci, Y., Andrews, A. T., IV, Sundaresan, S., Pannala, S., & O'Brien, T. (2008). Filtered two-fluid models for fluidized gas-particle suspensions. *AIChE Journal, 54*(6), 1431–1448.
Igci, Y., & Sundaresan, S. (2011). Constitutive models for filtered two-fluid models of fluidized gas–particle flows. *Industrial & Engineering Chemistry Research, 50*(23), 13190–13201.
Joseph, G. G., Leboreiro, J., Hrenya, C. M., & Stevens, A. R. (2007). Experimental segregation profiles in bubbling gas-fluidized beds. *AIChE Journal, 53*(11), 2804–2813.
Kaufmann, A., Moreau, M., Simonin, O., & Helie, J. (2008). Comparison between Lagrangian and mesoscopic Eulerian modelling approaches for inertial particles suspended in decaying isotropic turbulence. *Journal of Computational Physics, 227*(13), 6448–6472.
Khoe, G. K., Ip, T. L., & Grace, J. R. (1991). Rheological and fluidization behaviour of powders of different particle size distribution. *Powder Technology, 66*(2), 127–141.
Kunii, D., & Levenspiel, O. (1991a). Industrial applications of fluidized beds. In *Fluidization engineering*. pp. 15–59. Oxford: Butterworth-Heinemann.
Kunii, D., & Levenspiel, O. (1991b). Particle-to-gas mass and heat transfer. In *Fluidization engineering*. pp. 257–276. Oxford: Butterworth-Heinemann.
Laverman, J. A., Roghair, I., Annaland, M. V. S., & Kuipers, H. (2008). Investigation into the hydrodynamics of gas–solid fluidized beds using particle image velocimetry coupled with digital image analysis. *The Canadian Journal of Chemical Engineering, 86*(3), 523–535.
Li, T., Gopalakrishnan, P., Garg, R., & Shahnam, M. (2012). CFD–DEM study of effect of bed thickness for bubbling fluidized beds. *Particuology, 10*(5), 532–541.
Li, T., Grace, J., & Bi, X. (2010). Study of wall boundary condition in numerical simulations of bubbling fluidized beds. *Powder Technology, 203*(3), 447–457.
Liang, Y., Zhang, Y., Li, T., & Lu, C. (2014). A critical validation study on CPFD model in simulating gas–solid bubbling fluidized beds. *Powder Technology, 263*, 121–134.
Loha, C., Gu, S., De Wilde, J., Mahanta, P., & Chatterjee, P. K. (2014). Advances in mathematical modeling of fluidized bed gasification. *Renewable and Sustainable Energy Reviews, 40*, 688–715.
Lu, L., Benyahia, S., & Li, T. (2017). An efficient and reliable predictive method for fluidized bed simulation. *AIChE Journal, 63*(12), 5320–5334.
Lu, L., Gopalan, B., & Benyahia, S. (2017). Assessment of different discrete particle methods ability to predict gas-particle flow in a small-scale fluidized bed. *Industrial & Engineering Chemistry Research, 56*(27), 7865–7876.
Lu, L., Morris, A., Li, T., & Benyahia, S. (2017). Extension of a coarse grained particle method to simulate heat transfer in fluidized beds. *International Journal of Heat and Mass Transfer, 111*, 723–735.
Monazam, E. R., Breault, R. W., Weber, J., & Layfield, K. (2017). Elutriation of fines from binary particle mixtures in bubbling fluidized bed cold model. *Powder Technology, 305*, 340–346.
Ozel, A., Kolehmainen, J., Radl, S., & Sundaresan, S. (2016). Fluid and particle coarsening of drag force for discrete-parcel approach. *Chemical Engineering Science, 155*, 258–267.
Patankar, N. A., & Joseph, D. D. (2001). Modeling and numerical simulation of particulate flows by the Eulerian–Lagrangian approach. *International Journal of Multiphase Flow, 27*(10), 1659–1684.
Peng, Z., Doroodchi, E., Alghamdi, Y., & Moghtaderi, B. (2013). Mixing and segregation of solid mixtures in bubbling fluidized beds under conditions pertinent to the fuel reactor of a chemical looping system. *Powder Technology, 235*, 823–837.
Popoff, B., & Braun, M. (2007). A lagrangian approach to dense particulate flows. In *Proceedings of the ICMF 2007, 6th International Conference on Multiphase Flow*.
Sánchez-Delgado, S., Marugán-Cruz, C., Soria-Verdugo, A., & Santana, D. (2013). Estimation and experimental validation of the circulation time in a 2D gas–solid fluidized beds. *Powder Technology, 235*, 669–676.
Schwartz, S. R., Richardson, D. C., & Michel, P. (2012). An implementation of the soft-sphere discrete element method in a high-performance parallel gravity tree-code. *Granular Matter, 14*(3), 363–380.
Sheikhi, A., Sotudeh-Gharebagh, R., Eslami, A., & Sohi, A. H. (2012). Sequential modular simulation of ethanol production in a three-phase fluidized bed bioreactor. *Biochemical Engineering Journal, 63*, 95–103.
Shi, Z., Wang, W., & Li, J. (2011). A bubble-based EMMS model for gas–solid bubbling fluidization. *Chemical Engineering Science, 66*(22), 5541–5555.
Snider, D. M., O'rourke, P. J., & Andrews, M. J. (1998). Sediment flow in inclined vessels calculated using a multiphase particle-in-cell model for dense particle flows. *International Journal of Multiphase Flow, 24*(8), 1359–1382.
Snider, D. M. (2007). Three fundamental granular flow experiments and CPFD predictions. *Powder Technology, 176*(1), 36–46.
Snider, D. M., Clark, S. M., & O'Rourke, P. J. (2011). Eulerian–Lagrangian method for three-dimensional thermal reacting flow with application to coal gasifiers. *Chemical Engineering Science, 66*(6), 1285–1295.
Subramaniam, S. (2013). Lagrangian–Eulerian methods for multiphase flows. *Progress in Energy and Combustion Science, 39*(2–3), 215–245.
Sun, G., & Grace, J. R. (1992). Effect of particle size distribution in different fluidization regimes. *AIChE Journal, 38*(5), 716–722.
Syamlal, M., Rogers, W., & OBrien, T. J. (1993). *MFIX documentation theory guide* No. DOE/METC-94/1004, USDOE Morgantown Energy Technology Center, WV, USA.
Third, J. R., Chen, Y., & Müller, C. R. (2016). Comparison between finite volume and lattice-Boltzmann method simulations of gas-fluidised beds: Bed expansion and particle–fluid interaction force. *Computational Particle Mechanics, 3*(3), 373–381.
Tsuji, Y., Kawaguchi, T., & Tanaka, T. (1993). Discrete particle simulation of two-dimensional fluidized bed. *Powder Technology, 77*(1), 79–87.
Van Wachem, B. G. M., Schouten, J. C., Van den Bleek, C. M., Krishna, R., & Sinclair, J. L. (2001). Comparative analysis of CFD models of dense gas–solid systems. *AIChE Journal, 47*(5), 1035–1051.
Wang, Q., Niemi, T., Peltola, J., Kallio, S., Yang, H., Lu, J., et al. (2015). Particle size distribution in CPFD modeling of gas–solid flows in a CFB riser. *Particuology, 21*, 107–117.
Xiong, Q., Madadi-Kandjani, E., & Lorenzini, G. (2014). A LBM–DEM solver for fast discrete particle simulation of particle–fluid flows. *Continuum Mechanics and Thermodynamics, 26*(6), 907–917.
Xu, J., Qi, H., Fang, X., Lu, L., Ge, W., Wang, X., et al. (2011). Quasi-real-time simulation of rotating drum using discrete element method with parallel GPU computing. *Particuology, 9*(4), 446–450.